

Fabric Evolution and Dilatancy within Anisotropic Critical State Theory Guided and Validated by DEM

R. Wang, Y. F. Dafalias, P. Fu, J. M. Zhang

July 29, 2019

International Journal of Solids and Structures

Disclaimer

This document was prepared as an account of work sponsored by an agency of the United States government. Neither the United States government nor Lawrence Livermore National Security, LLC, nor any of their employees makes any warranty, expressed or implied, or assumes any legal liability or responsibility for the accuracy, completeness, or usefulness of any information, apparatus, product, or process disclosed, or represents that its use would not infringe privately owned rights. Reference herein to any specific commercial product, process, or service by trade name, trademark, manufacturer, or otherwise does not necessarily constitute or imply its endorsement, recommendation, or favoring by the United States government or Lawrence Livermore National Security, LLC. The views and opinions of authors expressed herein do not necessarily state or reflect those of the United States government or Lawrence Livermore National Security, LLC, and shall not be used for advertising or product endorsement purposes.

Fabric Evolution and Dilatancy within Anisotropic Critical State Theory 1 Guided and Validated by DEM 2 Rui Wang¹, Yannis F. Dafalias ^{2,3,4}, Pengcheng Fu⁵, Jian-Min Zhang⁶ 3 4 ¹Assistant Professor, Department of Hydraulic Engineering, State Key Laboratory of Hydroscience and 5 Engineering, Tsinghua University, Beijing, 100084, China. E-mail: wangrui 05@mail.tsinghua.edu.cn. 6 ²Distinguished Professor, Dept. of Civil and Environmental Engineering, Univ. of California, Davis, CA 7 95616, USA; E-mail: jfdafalias@ucdavis.edu 8 ³Emeritus Professor, Dept. of Mechanics, School of Applied Mathematical and Physical Sciences, National Technical Univ. of Athens, Zographou, 15773, Hellas; 10 ⁴Leading Research Scientist, Institute of Thermomechanics, Czech Academy of Sciences, 18200 Praha 11 8, Czech Republic. 12 ⁵Staff Scientist, Atmospheric, Earth, and Energy Division, Lawrence Livermore National Laboratory, 13 Livermore, CA 94551, USA. E-mail: fu4@llnl.gov. ⁶Professor, Department of Hydraulic Engineering, State Key Laboratory of Hydroscience and 14 Engineering, Tsinghua University, Beijing, 100084, China. E-mail: zhangjm@mail.tsinghua.edu.cn. 15 16

17

19

20

21

22

23

24

25

26

27

28

29

30

31

32

33

34

Abstract

Fabric, expressed by means of an evolving deviatoric fabric tensor F, plays a very important role in the anisotropic mechanical response of granular materials. The Anisotropic Critical State Theory (ACST) addresses fabric anisotropy by rendering dilatancy a function of F, in addition to other state variables. In this paper, 3D DEM is used to guide the specific definition of F, the formulation of its continuum evolution equation and its effect on anisotropic dilatancy within ACST. DEM provides stressratio and shear strain variations as input for ACST analytical calculations of evolving fabric tensor and dilatancy, which are then favourably compared with totally independent direct measurements of these quantities by DEM. Dilatancy is shown to be strongly affected by the contact normal-based fabric tensor F, whose evolution is best described by a continuum equation within ACST that also includes a particle orientation-based fabric quantity. The aforementioned favourable comparison of the results for fabric tensor and dilatancy obtained independently by ACST and DEM, confirms the validity of the core framework of ACST irrespective of any constitutive model that addresses the deviatoric stress-strain relations.

35

Keywords: Anisotropic critical state theory, fabric evolution, dilatancy, DEM

37

36

1. Introduction

38

39

40

41

42

43

44

45

46

47

48

49

50

51

52

53

54

55

56

57

58

59

Fabric and its evolution play a very important role in the mechanical response of granular materials and are, therefore, an integral component of the corresponding constitutive relations that address the so-called fabric anisotropy. Fabric quantification is commonly achieved by the means of a fabric tensor F which can be defined by and associated with the statistical distribution of the orientation of unit vectors along the major axis of elongated particles, contact normal directions, void vectors, scan-line directions or other micromechanical oriented entities. In most continuum theories the notion of a fabric tensor is not necessarily associated with a specific microscopic entity. While F has been included in various ways into several constitutive relations in the past (e.g. Tobita, 1987; Oda, 1993; Wu, 1998; Wan and Guo, 2001, 2004; Li and Dafalias, 2002; Dafalias et al., 2004; Yao et al., 2017; Ueda and Iai, 2018), its fundamental role as an element of a general framework for constitutive relations rather than specific constitutive models, was only recently recognized with the development of Anisotropic Critical State Theory (ACST) by Li and Dafalias (2012). ACST extends the classical Critical State Theory (CSR) (Roscoe et al., 1958; Schofield and Wroth, 1968) that did not consider fabric. ACST achieves two tasks. First, it enriches the two conditions of CST regarding stress and void ratios at Critical State (CS) by a third, related to the CS value of F in combination with the deviatoric plastic strain rate unit norm direction n. This combination is expressed by means of the Fabric Anisotropy variable (FAV) A=F:n, where ":" signifies the trace of the product of the adjacent tensors. With a proper normalization of the norm of \mathbf{F} , the third CS condition yields $A = A_c = 1$. In the process the very important rate equation of evolution for \mathbf{F} must be formulated in a way that satisfies the foregoing third CS condition. The foregoing conclusion was motivated by DEM results in relation to a void based (Li and Li, 2009) and a contact normal based (Fu and Dafalias, 2011) fabric tensor. It was later shown by Theocharis et al. (2017, 2019), that this third condition must be added to the two classical conditions of the CST in order to render all three of them both necessary and sufficient for reaching and maintaining CS without the additional assumption of fixity of the plastic strain rate direction (or stress direction) at CS implied in classical CST.

The second task of ACST was to render the phase transformation stress ratio and the ensuing dilatancy D, function of A, hence of \mathbf{F} , in addition to dependence on void ratio e and mean pressure p by means of the state parameter ψ (Been and Jefferies, 1985). The ACST is mainly a theory on fabric dependent dilatancy, without addressing the deviatoric stress-strain response that is delegated to any chosen specific constitutive model formulated within the premises of ACST. By such dependence of D on \mathbf{F} via A, it was possible to simulate the strongly anisotropic response of samples loaded at various directions in regard to fabric tensor, as initially shown by Li and Dafalias (2012), followed by numerous subsequent papers with various constitutive models within ACST (Gao et al., 2014; Li and Dafalias, 2015; Woo and Salgado, 2015; Zhao and Gao, 2016; Petalas et al., 2018; Papadimitriou et al., 2018; Yang et al., 2018). The dependence of phase transformation stress ratio, thus of dilatancy D, on fabric, has been investigated earlier by Wan and Guo (2001, 2004) but differs fundamentally from the

present development within ACST in two aspects. First, the assumed evolution of F is not related to its convergence with specific CS values, as demonstrated by numerous DEM studies, that constitutes the basis for showing the uniqueness of the Critical State Line (Li and Dafalias, 2012). Second, the dilatancy D depends not only on F, e and p as in ACST, but also on a modified cumulative plastic shear strain that given a sample is impossible to measure, as opposed to F, e and p that can all be measured in principle. While the continuum theory embodied by a typical constitutive model for sands within ACST yielded very good simulations based on the use of a generic macroscopic F and its evolution, it still remains an open question as to which microscopically defined fabric tensor is more appropriate for constructing the macroscopic entity F entering ACST. Furthermore, the validity of the fundamental macroscopic analytical relations of ACST for the evolution of F and the dependence of dilatancy on F via A, has been confirmed indirectly by successful simulations of data by the various models of all the aforementioned references, but not directly in terms of measured or computed grainscale quantities. What has been done so far by the means of DEM (there are numerous works with DEM addressing fabric but here only those related to ACST are considered), is to confirm concepts used in ACST such as the convergence of fabric tensor with **n** at CS and the anisotropic response of granular assemblages if loaded at various orientations with different Lode angles as well as the effect of fabric anisotropy on issues of controllability and instability (Li and Li, 2009; Fu and Dafalias, 2011; Guo and Zhao, 2013; Zhao and Guo, 2013, Yang and Wu, 2016; Wang et al., 2017; Shi and Guo, 2018; Lashkari at al., 2019). In some very recent papers, the DEM confirmation

82

83

84

85

86

87

88

89

90

91

92

93

94

95

96

97

98

99

100

101

102

103

of the analytical relations of ACST was done half-way only, as follows. In Hu et al. (2019) and Yuan et al. (2019) a rate equation of evolution for \mathbf{F} , active even if no plastic deformation takes place, was validated versus DEM measurements of a contact normal based \mathbf{F} . However, the dilatancy was not rendered function of \mathbf{F} , hence, denying one of the most important features of ACST, namely that of a fabric anisotropy dependent dilatancy. In Wang et al. (2019a) the task was to confirm the validity of the analytical dependence of dilatancy D on \mathbf{F} via A, as postulated by ACST. Hence, DEM loadings at various orientations were carried out calculating stress, strain, fabric tensor and dilatancy, and then using as input the DEM calculated fabric tensor \mathbf{F} into the ACST analytical expression for D in terms of \mathbf{F} and other entities, favorable comparison of the analytically calculated values of D with those obtained directly by DEM during the loading sequence till critical state failure, was obtained.

It follows that up until now there is no DEM confirmation of both main ACST analytical expressions for the rate of evolution of **F** and the dependence of *D* on **F** via *A*. The present paper comes to cover exactly this missing link. The procedure is very simple and straightforward. As in Wang et al. (2019a), a DEM loading sequence at various orientations in regard to fabric, first drained and then undrained, is carried out, and stress, deviatoric strain, fabric tensor, dilatancy and volume change are recorded. Subsequently, instead of using as input to ACST the DEM calculated **F**, as done in Wang et al. (2019a), appropriate rate equations of evolution within ACST are used to calculate analytically **F** as an evolving internal variable, which then is used to calculate *D* by the ACST analytical expression of the latter. In other words, unlike what has

happened in prior publications, the calculations of F and D by means of analytical relations within ACST are carried out totally independently from the DEM calculated **F** and D, and subsequently compared with them. The only input to ACST from DEM is the stress and deviatoric strain at each step of the loading process, that as mentioned before are delegated to be obtained by an appropriate constitutive model. This approach eliminates the need to rely the comparison on a specific constitutive model within ACST and enables to focus on evolving fabric and dilatancy, the key features of ACST. In the process of carrying out this task, other issues will also be addressed. One will be the examination of the performance of various rate equations for F proposed in past works, including their effect on dilatancy D. Another will be the sensitivity of the dependence of D on the "exact" calculation of F. This DEM based investigation will yield new insight for the optimal formulation of a novel continuum fabric tensor evolution equation appropriate for ACST, involving contact normal and particle orientation-based fabric tensors in combination. Overall it will be the most independent, direct grain-level validation and calibration of ACST done so far by means of DEM.

141

142

143

144

145

146

147

148

140

126

127

128

129

130

131

132

133

134

135

136

137

138

139

2. DEM test scheme and typical observations

2.1 Stress-strain and dilatancy calculations by means of DEM

The open source code *Yade* (Šmilauer et al., 2015) is used in this study for 3D DEM numerical testing, to provide a basis for the formulation and validation of fabric evolution and dilatancy equations in ACST. Sixteen drained constant-mean effective stress (*p*) triaxial tests (meaning "true-triaxial tests" in this work) with various intermediate principal stress coefficient *b* values (0, 0.25, 0.5, 0.75, and 1)

corresponding to various Lode angles, are conducted on specimens with various initial void ratios ($e_0 = 0.690\pm0.005$, 0.656 ± 0.005 , and 0.570 ± 0.005) and initial fabric orientations. Two undrained triaxial compression tests are also conducted on two specimens with the same void ratio ($e_0 = 0.655$) but different initial fabric orientations, as listed in Table 1. Specimens with different initial fabric orientations are generated by altering the bedding plane angle φ (0°, 30°, 60°, 90°), i.e. the angle between particle deposition direction and the major principal stress axis (Fig. 1 (a)). Note in this study, the minor principal stress is always parallel to the bedding plane.

Elongated particles with aspect ratio of 1.5:1 are used in this study for pronounced anisotropic behaviour. The details of the particle and contact law specifications have been reported in Wang et al. (2019 a). Constant *p* triaxial loading is achieved by servocontrolled loading on rigid frictionless walls, while undrained triaxial loading is achieved by enforcing a constant-volume condition, which has been successfully applied in several studies (Kuhn et al., 2014; Wang et al., 2016; Wang et al., 2019 b). The specimens are consolidated under 100kPa confining stress. The homogeneity of the specimens after consolidation are verified rigorously by examining the consistency of stress and density in different regions within the specimen. Largely uniform deformation without the appearance of significant global shear bands and strain localization is observed in the tests, verified via the method proposed by Wang et al. (2017). During loading, the inertial number *I* is restricted within 10-5, to achieve quasistatic conditions (MiDi GDR, 2004).

 Table 1. DEM test scheme

Test	Initial void	Intermediate	Bedding plane	Looding
number	ratio e ₀	principal stress	angle φ (°)	Loading

		coefficient b		
1	0.693	0	0	
2	0.685	0	30	drained, constant p
3	0.692	0	60	
4	0.690	0	90	
5	0.655	0	0	
6	0.658	0	30	drained, constant p
7	0.654	0	60	
8	0.655	0	90	
9	0.658	0.25	0	
10	0.656	0.5	0	drained, constant p
11	0.658	0.75	0	
12	0.656	1	0	
13	0.570	0	0	
14	0.570	0	30	drained, constant p
15	0.570	0	60	
16	0.569	0	90	
17	0.655	0	0	undrained
18	0.655	0	90	undrained

In DEM, stress is computed as the per-volume summation of the tensor product of contact force vectors and corresponding contact branch vectors (Bagi, 1996). Strain is calculated from the displacements of particles at the vertices of a Delaunay tessellation of the granular assembly (Fu and Dafalias, 2012; Xue et al., 2019). Stress and strain are denoted positive in compression, following traditional soil mechanics sign conventions. The mean effective stress p is $\text{tr}(\sigma)/3$, where $\text{tr}(\sigma)$ is the trace of the effective stress tensor σ . The deviatoric stress q is $[3/2(\sigma-p\mathbf{I}):(\sigma-p\mathbf{I})]^{1/2}$, where \mathbf{I} is the second order identity tensor; $\eta=q/p$ is referred to as the deviatoric stress ratio. The volumetric strain ε_v is the trace $\text{tr}(\varepsilon)$ of the strain tensor ε , while the deviatoric strain ε_q equals $[2/3(\varepsilon-\varepsilon_v/3\mathbf{I}):(\varepsilon-\varepsilon_v/3\mathbf{I})]^{1/2}$. Corresponding definitions apply to strain rates. The dilatancy D is defined as the ratio of the volumetric to deviatoric plastic strain increments, i.e. $D=(d\varepsilon_v^p/d\varepsilon_q^p)$. The plastic strain increment $d\varepsilon^p$ is calculated by subtracting the elastic strain increment $d\varepsilon^p$ from the total strain increment following the procedure suggested by Wan and Pinheiro (2014) and Wang et al. (2019 a).

The stress-strain results from two typical drained DEM triaxial tests under b=0 on

specimens with e_0 =0.656±0.005, and bedding plane angle φ =0° and 90°, respectively, are presented in Fig. 1. Significant anisotropic behaviours are observed for the two specimens with different bedding plane angle φ . Fig. 1 (b) and (c) show that the specimen with φ =0° exhibits higher peak shear strength and stronger tendency to dilate compared with the specimen with φ =90°, though both specimens converge toward the same critical state in terms of deviatoric stress ratio η and void ratio e at large deviatoric strain, consistent with findings in the literature (Oda, 1972; Guo, 2008; Fu and Dafalias, 2011b; Tong et al., 2014; Yang et al., 2016; Cao et al., 2016; Wang et al., 2017).

The variations of dilatancy D with respect to η for the specimens in the two tests are directly compared in Fig. 1 (d). The specimen with $\varphi=90^\circ$ is significantly more contractive in the early stage of loading at low η . At higher η values, the D- η relationship converges towards the same point, denoted as the "critical state" in the figure, while the dilatancy at peak stress ratio, also called peak dilatancy (negative in dilation), is significantly greater in absolute value for the specimen with $\varphi=0^\circ$. At the critical state, D=0 at same critical stress ratio for both specimens, as expected from CST and its extension by ACST. Also observe that D=0 instantaneously during loading when η crosses the phase transformation, such crossing is indicated in the D- η plot of Fig. 1(d) by dashed circles; this happens at quite different values of η for the two specimens, smaller for the specimen with $\varphi=0^\circ$. The comparison of the stress-strain behaviour of the specimens with $\varphi=0^\circ$ and $\varphi=90^\circ$ is analogous to that between a denser and a looser specimen, respectively.

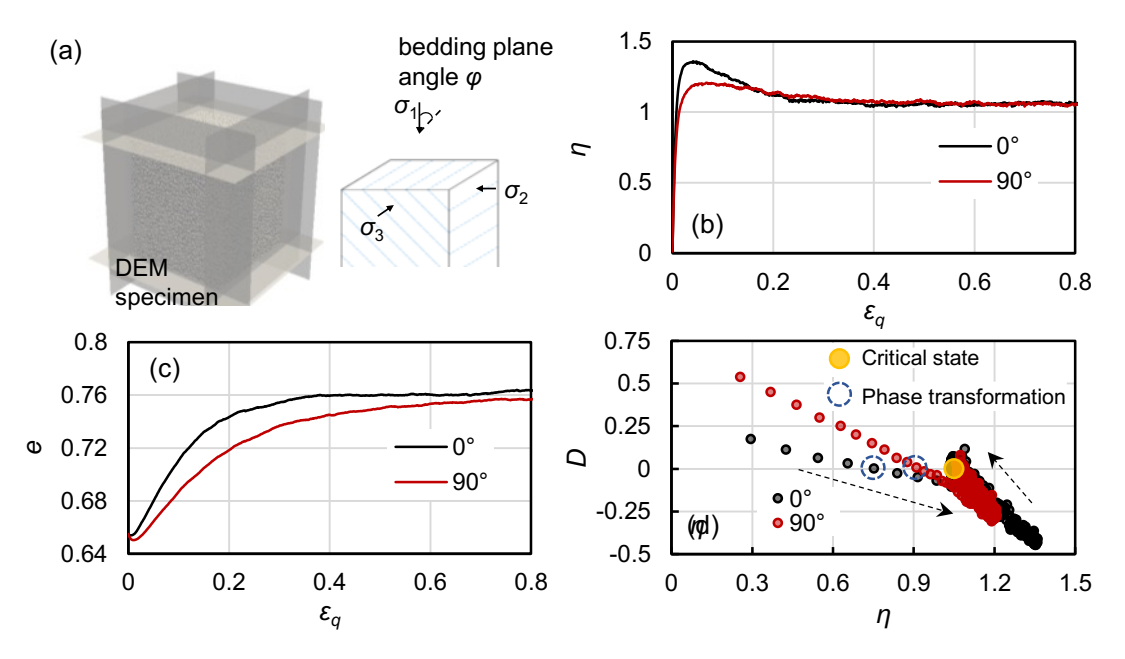


Fig. 1 Typical drained DEM tests on two specimens with e_0 =0.656±0.005, and bedding plane angle φ =0° and 90°: (a) DEM specimen and loading schematic; (b) deviatoric stress ratio η - deviatoric strain ε_q ; (c) void ratio e- ε_q ; (d) dilatancy D- η .

2.2 Contact normal and particle orientation-based fabric tensors

Denoting, henceforth, by superscript * a fabric tensor calculated by means of DEM, the deviatoric fabric tensor \mathbf{F}^* can be calculated as (Satake, 1982):

$$\mathbf{F}^* = \frac{1}{(1+e)} \left(\frac{1}{N} \sum_{k=1}^{N} \mathbf{v}^k \otimes \mathbf{v}^k - \frac{1}{3} \mathbf{I} \right)$$
 (1)

where N is the number of contacts, \mathbf{v}^k is the unit norm vector attributed to the k^{th} grain scale entity used to define the fabric tensor, e is the void ratio. The term 1+e is introduced to define a per-volume measure of fabric tensor for thermodynamic consistency required for the continuum definition of fabric as an internal variable (Li and Dafalias, 2015).

Motivated by the notion of Fabric Anisotropy Variable (FAV) $A=\mathbf{F}:\mathbf{n}$ introduced in ACST, two quantities will be used to evaluate fabric anisotropy. First is the norm of the deviatoric fabric tensor $F^*=||\mathbf{F}^*||=\sqrt{\mathbf{F}^*:\mathbf{F}^*}$ that measures the intensity of fabric

anisotropy. Second is the quantity $N^* = (\mathbf{F}^* / F^*) \cdot \mathbf{n}$, which is independent of the norm and measures the orientation of the fabric tensor with respect to \mathbf{n} , since \mathbf{F}^*/F^* is a unit norm deviatoric tensor along \mathbf{F}^* . Based on the foregoing definitions it follows that A^* $= \mathbf{F}^* : \mathbf{n} = F^* N^*$. It must be mentioned that in what follows in this section the DEM calculated norms are not normalized by their CS values, hence, the A* does not attain unity at CS with no effect whatsoever on the basic premises of ACST (Dafalias, 2016). Common examples of grain-scale features used to define the fabric tensor include the contact normal vector and the particle orientation vector, which yield the contact normal fabric tensor \mathbf{F}_{c}^{*} and particle orientation fabric tensor \mathbf{F}_{p}^{*} , respectively. For the two typical drained DEM tests in Fig. 1, F_c^* and N_c^* of the contact normal fabric tensor and F_p^* and N_p^* of the particle orientation fabric tensor are plotted in Fig. 2 against both deviatoric strain ε_q and deviatoric stress ratio η . At the initial state, the norms $F^*_{\ c}$ and F_{p}^{*} are the same for the two specimens since they are independent of orientation, while $N_{\rm c}^*$ and $N_{\rm p}^*$ are distinctly different, reflecting the difference in bedding plane angle φ . The initial evolution of the contact normal fabric is faster than that of the particle orientation fabric. The specimen with $\varphi=0^{\circ}$ experiences a peak F_{c}^{*} . For the two tests, the contact normal fabric tensor reaches the same stable state after $\varepsilon_q > 0.4$, while the particle orientation fabric tensor converges to the same stable state after $\varepsilon_q > 0.7$ (Fig. 2 (a) and (c)). At $\varepsilon_q > 0.7$, stress, void ratio, and fabric anisotropy all reach their respective constant values, confirming the reaching of critical state. At the critical state, $N_{c}^{*}=1$ while F_{c}^{*} is unique under the same loading condition, complying with the basic hypothesis of ACST. For the particle orientation fabric, F_p^* is also unique at the critical

223

224

225

226

227

228

229

230

231

232

233

234

235

236

237

238

239

240

241

242

243

244

state under the same loading condition, though $N_p^* = -1$, since $\mathbf{F}_p^* / F_p^* = -\mathbf{F}_c^* / F_c^*$ at CS.

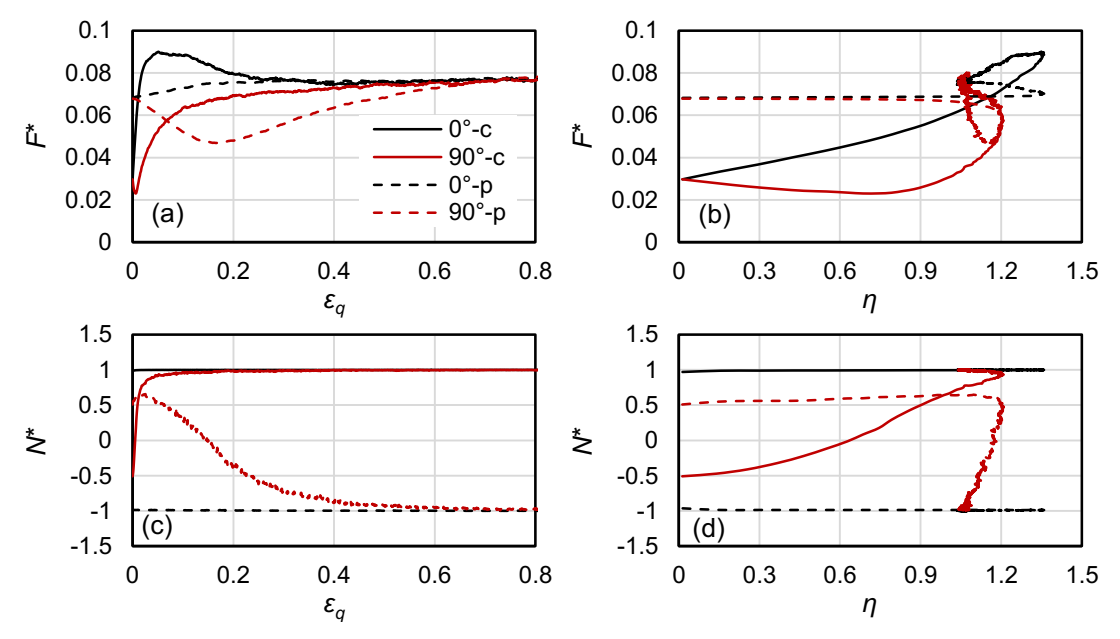


Fig. 2 Contact normal and particle orientation fabric evolution in drained DEM tests on two specimens with e_0 =0.656±0.005, and bedding plane angle φ =0° and 90°: (a) F^* - ε_q ; (b) F^* - η ; (c) N^* - ε_q ; (d) N^* - η ; N^* =(\mathbf{F}^* :n)/ F^* is a measure of the relative orientation of the fabric tensor \mathbf{F}^* and unit-norm deviatoric tensor-valued loading direction \mathbf{n} . c and \mathbf{p} in the legend denote contact normal fabric and particle orientation fabric, respectively.

A first hint as to which grain level-defined fabric tensor may be considered best suited for representing the generic notion of such tensor in ACST, can be obtained from Fig. 2. In Fig. 2 (b) and (d), the contact normal fabric tensor evolves continuously from the initiation of loading, and N^*_c of the two specimens becomes very close at high η , e.g. at $\eta > 1$, similar to the convergence of $D-\eta$ relationship at high η as seen in Fig. 1(d). In comparison, the particle orientation fabric evolves significantly only as peak η is reached. Therefore, as suggested in Wang et al. (2019a), it seems that the contact normal based fabric tensor is better suited to address the dilatancy dependence on fabric in a way that will be addressed in the sequel.

3. Fabric evolution and dilatancy in ACST motivated by DEM results

3.1 Fabric dependence of dilatancy within ACST

261

262

281

282

283

In the ACST framework (Li and Dafalias, 2012), the volume-related anisotropic behaviour of granular materials is addressed by introducing the role of a deviatoric fabric tensor **F** via the aforementioned Fabric Anisotropy Variable (FAV) A=**F**:**n** into dilatancy as follows. A new state variable, the Dilatancy State Parameter (DSP) ζ combines both the classical State Parameter (SP) $\psi = e - e_c$ by Been and Jefferies (1985), with e_c the critical state void ratio at current p, and FAV A in its definition as follows:

$$\zeta = \psi - \hat{e}_{A}(A - 1) \tag{2}$$

where \hat{e}_A can be a function of the void ratio e and/or the mean effective stress p (Li and Dafalias, 2012). The ζ substitutes for ψ in the definition of a variable with ψ phase transformation line (or dilatancy stress ratio), an idea originally proposed by Manzari and Dafalias (1997). Therefore, a dilatancy based on the essence of Rowe's dilatancy theory (Rowe 1962), can be expressed as:

$$D = d(M \exp(m\zeta) - \eta) \tag{3}$$

where M is the critical state stress ratio, d and m are material parameters or functions that are often assumed to be constant (e.g. Dafalias and Manzari, 2004; Wang et al., 279 2014). The exponential dependence of dilatancy stress ratio on ζ is adopted from the 280 corresponding expression in Li and Dafalias (2000) for ψ .

Normalization of **F** by its critical state norm F_{crit} , which depends on the Lode angle, yields a third condition $A=A_c=1$ when reaching critical state, that in combination with $\psi=0$ yields $\zeta=0$ and D=0 at critical state according to Eqs. (2) and (3). The foregoing

normalization of a DEM calculated \mathbf{F}^* as in Eq. (1) by its norm F^*_{crit} will henceforth be adopted, hence, hereafter, a fabric tensor refers to its normalized version either as a continuum variable within ACST or as a DEM calculated entity, i.e. $\mathbf{F} = \mathbf{F}^*/F^*_{\text{crit}}$, unless specifically otherwise indicated.

A key step in ACST is the formulation of the rate evolution equation of **F** towards its critical state value. Li and Dafalias (2012) proposed an equation of **F** that reads:

290
$$\dot{\mathbf{F}} = \langle \lambda \rangle c(\mathbf{n} - r\mathbf{F}) = \langle \lambda \rangle \frac{c_c}{r} (\mathbf{n} - r\mathbf{F}) = \langle \lambda \rangle c_c (\frac{1}{r} \mathbf{n} - \mathbf{F})$$
 (4)

where $\dot{\mathbf{F}}$ is the rate of evolution for \mathbf{F} ; λ within the Macauley brackets <> is the plastic multiplier which can be expressed as $<\lambda>=|\dot{\varepsilon}_q^p|$ in terms of the plastic deviatoric strain rate norm. With no loss of generality $c_c=rc$ was set in Eq. (4) with c_c and r constitutive parameters or functions, the former dictating the pace of fabric evolution and the latter its peak value. The specific form of those two parameters were not addressed in the original ACST formulation (Li and Dafalias, 2012).

In order to compare results obtained by DEM and ACST the following procedure is adopted. The input to ACST from DEM calculations consists of a given stress ratio η , its increment and the deviatoric plastic strain increment. A typical example of such input was presented in Fig. 1 (b), but it is not necessary to show such input in all subsequent cases. The output from ACST is obtained as follows: first, λ is identified based on the deviatoric plastic strain increment, then the fabric tensor is updated by Eq.(4) using the **n** defined by the provided plastic strain increment tensor, followed by calculation of the Fabric Anisotropy Variable (FAV) A and the ensuing Dilatancy State Parameter (DSP) ζ from Eq.(2). Then dilatancy D is calculated from Eq. (3) that in turn

is used to calculate the volumetric strain and ensuing void ratio changes based on the deviatoric plastic strain increment provided. These steps are then repeated. The initial values of void ratio and fabric tensor, and the corresponding critical state void ratio used in the ACST calculations are also obtained from DEM measurements as a virtual substitute of real experimental data. For the drained constant p=100 kPa triaxial tests, $e_c=0.761$ is determined from the mean void ratio of sixteen drained tests, at 0.8 deviatoric strain. For the triaxial tests with b=0, M=1.06 is determined from the mean deviatoric strain. For the fourteen tests with b=0, at 0.8 deviatoric strain. For simplicity, it is assumed in this study that d, m, and \hat{e}_A in Eqs. (2) and (3) are constants.

3.2 Performance of two simple fabric evolution formulations

ACST does not specify which microscopically defined fabric tensor is more appropriate for \mathbf{F} in Eqs. (2)-(4). Based on the observations from DEM results in this study (Fig. 1-2), it would be reasonable to simulate the evolution of the contact normal fabric tensor \mathbf{F}_c with various forms of Eq. (4) and use \mathbf{F}_c to address the anisotropic dilatancy of granular materials via Eqs. (2) and (3). One may rename in that case the FAV A entering Eq. (2) as A_c = \mathbf{F}_c : \mathbf{n} .

In the simplest form of Eq. (4) one considers c_c to be constant, and r=1 to guarantee that at critical state Eq. (4) results in $\dot{\mathbf{F}}_c = 0$ and $\mathbf{F}_c = \mathbf{n}$; thus, one can write:

$$\dot{\mathbf{F}}_{c} = <\lambda > c_{c}(\mathbf{n} - \mathbf{F}_{c}) \tag{5}$$

This simplified rate equation only requires one parameter to depict the evolution of the fabric tensor. While it guarantees the eventual convergence of the fabric tensor towards its critical state, Eq. (5) does not reflect the peak in F_c^* observed for the

specimen with $\varphi=0^\circ$ in Fig. 2. To capture this peak behaviour, the parameter r in Eq. 4 should be able to become smaller than unity before the critical state (Li and Dafalias, 2012), instead of being constant as in Eq. (5). Yang et al. (2018) suggested incorporating dilatancy D in r of Eq. (4) in the form of r=1+D. This achieves an evolving r that can be smaller than 1 for dense material with D<0 in the dilative state while guaranteeing r=1 at the critical state where D=0. Extending the foregoing suggestion, a similar approach is tested in this study using the following equation:

335
$$\dot{\mathbf{F}}_{c} = \langle \lambda \rangle c_{c} \left(\frac{1}{(1 + c_{cd}D)} \mathbf{n} - \mathbf{F}_{c} \right)$$
 (6)

where a new parameter $c_{\rm cd}$ is introduced to provide better control of the peak contact normal fabric norm; $c_{\rm cd} = 0$ reduces Eq. (6) to Eq. (5).

Using Eqs. (2), (3), (5) and (6), with parameters listed in Table 2, fabric and void ratio evolution results can be obtained independently from DEM under the same initial and loading conditions. The value of the parameter c_{cd} in Eq. (6) is set at 0.3, while the other parameters for the simulations using Eqs. (5) and (6) are exactly the same (Table 2). Fig. 3 plots the ACST and DEM contact normal fabric norm evolution results for the two tests on specimens with e_0 =0.656±0.005, and bedding plane angle φ =0° and 90°, under b=0.

It is evident that even the simplest form of Eq. (5) can capture the fundamental behaviour of fabric tensor evolution towards its critical state values, irrespective of the initial fabric, because this is built into the basic formulation. However, the difference in the F_c - ε_q plots resulting from Eq. (5) for the two specimens with different φ , is significantly underestimated compared to the DEM results, as seen in Fig. 3 (a).

Although the evolution of the contact normal fabric in the F_c - η space seems to be reasonably well captured with Eq. (5) at low η values, it is observed that the peak of fabric norm for φ =0° observed in DEM results is not achieved (Fig. 3 (a) and (b)), and significant discrepancies between ACST and DEM results develop at high η . Fig. 3 (c) and (d) show that by introducing dilatancy into the rate Eq. (6), one can achieve a good representation of the fabric norm peak for dense granular materials, however, the difference in fabric evolution in the F_c - ε_q space for the two specimens with different φ is still poorly represented.

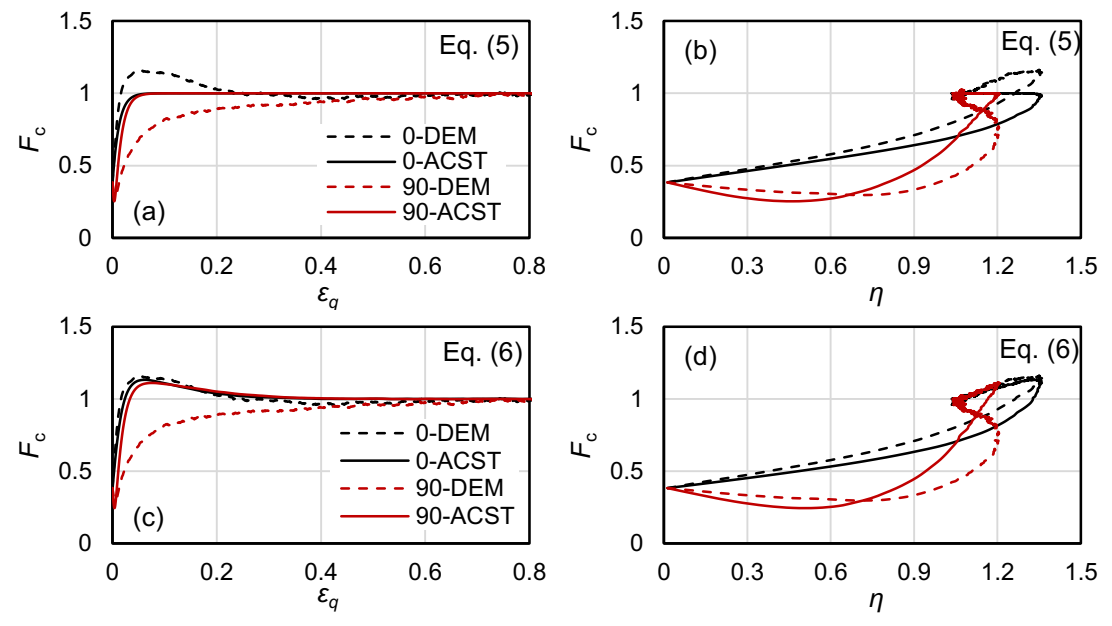


Fig. 3 Contact normal fabric evolution results from drained DEM tests and ACST simulations using Eq. (5) and Eq. (6), for specimens with e_0 =0.656±0.005, and bedding plane angle φ =0°and 90°: (a) F_c - ε_q from Eq. (5); (b) F_c - η from Eq. (5); (c) F_c - ε_q from Eq. (6); (d) F_c - η from Eq. (6).

The discrepancy between fabric evolution in the F_c - ε_q space in ACST calculations using Eqs. (5) and (6) and DEM has important consequences in volumetric behaviour. It leads to significant underestimation of anisotropy differences in void ratio development, as plotted in Fig. 4. The DEM results show that the specimen with φ =0° is much more dilative than that with φ =90° for ε_q between 0.1-0.4 (Fig. 4), while the

difference between the two tests based on ACST is much smaller during the entire loading process, using either Eq. (5) or (6), which cannot be overcome simply by adjusting the parameters in Table 2. For example, if a smaller c_c value is adopted, although the difference between the fabric tensor norms of the two tests with different φ would persist till later during loading, the overall fabric evolution would become much slower compared to the DEM results. This suggests that even if the peak behaviour of fabric is captured by Eq. (6), some key ingredient is still missing.

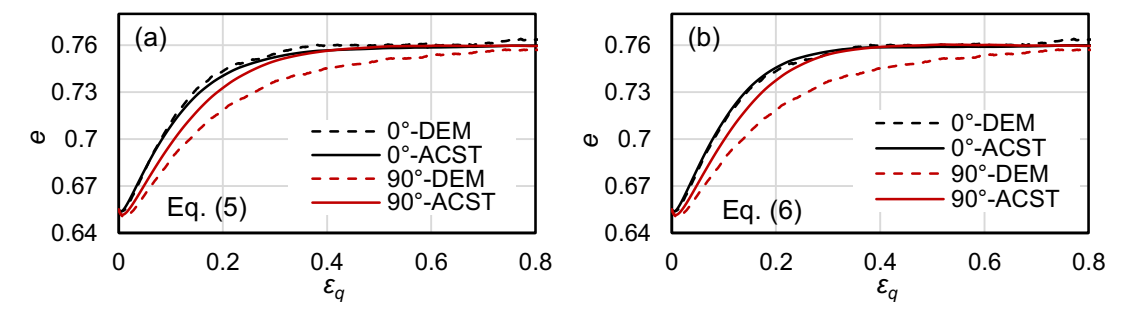


Fig. 4 Void ratio development results from drained DEM tests and ACST simulations using Eq. (5) and Eq. (6), for specimens with e_0 =0.656±0.005, and bedding plane angle φ =0°and 90°: (a) e- ε_q from Eq. (5); (b) e- ε_q from Eq. (6).

Table 2. Input parameters for various fabric evolution equations in ACST

Parameter	Eq. (5)	Eq. (6)	Eqs. (7) and (8)
$\hat{m{e}}_{_A}$	0.11	0.11	0.11
d	0.44	0.44	0.44
m	10	10	10
Cc	80	80	80
\mathcal{C} cd	/	0.3	0.55
β	/	/	0.3
$c_{ m p}$	/	/	4.5
$\mathcal{C}_{ ext{pd}}$	/	/	0.2

4. A combined fabric evolution equation and comparisons with DEM

4.1 Theoretical development

Wang et al. (2017) suggested that various fabric tensors defined based on different grain scale quantities may be inter-dependent. In the two idealized configurations of a

granular material in Fig. 5, the contact normal fabric tensors are the same (isotropic) according to Eq. (1), while the particle orientation fabric tensors are clearly different. Under the same vertical compression loading, the evolution of the contact normal fabric would no doubt be different, influenced by the difference in particle orientation fabric.

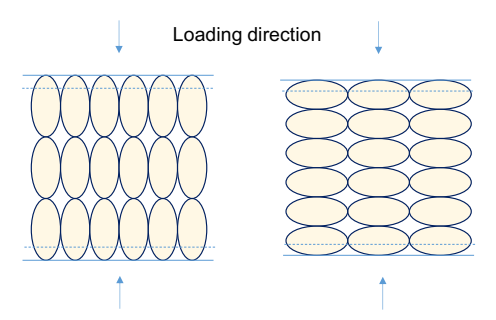


Fig. 5 Illustration of the possible influence of particle orientation fabric on the evolution of the contact normal fabric.

It is hence plausible to make the hypothesis that the particle orientation fabric tensor, which converges with its critical state at a much slower rate compared with the contact normal fabric (Fig. 2), can delay the evolution of the contact normal fabric at relatively large strains. The lack of reference to the particle orientation fabric in Eqs. (5) and (6) may be the reason for their tendency to overestimate the convergence rate of fabric towards the critical state. Therefore, the influence of the particle orientation fabric on contact normal fabric evolution should be considered when formulating the rate equation of \mathbf{F}_c . To this extent, a combined formulation for fabric evolution is presented in the following equations for both contact normal and particle orientation-based fabric tensors:

 $\dot{\mathbf{F}}_{c} = \langle \lambda \rangle c_{c} \left(\frac{\exp(-\beta(1 + A_{p}))}{1 + c_{cd}D} \mathbf{n} - \mathbf{F}_{c} \right)$ (7)

$$\dot{\mathbf{F}}_{p} = \langle \lambda \rangle c_{p} \left(\frac{1}{1 + c_{pd}D} \mathbf{n} + \mathbf{F}_{p} \right)$$
 (8)

where it is clear from Eq. (7) what is the expression for the coefficient r of the original Eq. (4) proposed in Li and Dafalias (2012). The influence of the particle orientation fabric is incorporated via the relevant FAV $A_p = \mathbf{F_p} : \mathbf{n}$, with the positive parameter β used to adjust the amount of influence A_p imposes on the evolution of \mathbf{F}_c . The parameter β is expected to be related to particle elongation or aspect ratio R and other factors. For spherical particles, where particle orientation is non-existent resulting in isotropic fabric, hence, $\mathbf{F}_p = \mathbf{0}$ and $A_p = 0$, β should be set equal to 0 so that $\mathbf{F}_c = \mathbf{n}$ from Eq. (7) at critical state where D = 0; in fact $\beta = 0$ reduces Eq. (7) to the form of Eq. (6). The case of spherical particles deserves a more detailed consideration addressed in the Appendix. The \mathbf{F}_p evolution Eq. (8) is similar to that of \mathbf{F}_c in Eq. (6), with parameters c_p controlling the pace of evolution and c_{pd} the peak behaviour related to D. The expression + \mathbf{F}_p instead of $-\mathbf{F}_p$ is used in Eq. (8), because at critical state one has \mathbf{F}_p =- \mathbf{n} , shown in Fig. 2, as opposed to $\mathbf{F}_c = \mathbf{n}$ for the contact normal fabric. Compared with the simplest form of Eq. (5), the present combined formulation requires four additional parameters b, c_{cd} , c_p and c_{pd} . Using Eqs. (7) and (8) in conjunction with Eqs. (2) and (3), with parameters listed in Table 2, one can obtain the simulations of fabric tensors evolution and dilatancy for the various categories of tests in Table 1. Such simulations show in general a satisfactory agreement with DEM results. These 18 tests include drained tests on specimens with different bedding plane angles and initial void ratios, drained tests with different intermediate principal stress coefficients b, and undrained tests on specimens

with different bedding plane angles. A description of these simulations follows.

403

404

405

406

407

408

409

410

411

412

413

414

415

416

417

418

419

420

421

422

423

424

4.2 Simulations of DEM drained tests with different bedding plane angle φ

425

426

427

428

429

430

431

432

433

434

435

436

437

438

439

440

441

442

443

444

445

446

The ACST results for contact normal fabric evolution calculated with Eqs. (7) and (8) are compared with the DEM test results in Fig. 6, for the four specimens with e_0 =0.656±0.005, and bedding plane angle φ =0°, 30°, 60°, and 90°, under b=0. A distinct feature observed in the ACST results using the combined fabric evolution formulation is that the difference in contact normal fabric norm between the specimens with different φ is preserved until much larger ε_q , due to the dependence of \mathbf{F}_c on \mathbf{F}_p . Better simulation of fabric evolution in the F_c - η space is also achieved at at high η values compared with the simulations in Fig. 3. The peaks in F_c for the two specimens with $\varphi=0^{\circ}$ and 30° are captured, while the general difference in the evolution of F_c during the entire loading process for the four specimens with different bedding plane angles is reflected in Figs. 6 (a) and (b). The calculated contact normal fabric tensor orientation, represented by N_c , also shows good agreement with DEM results. In the N_c - ε_q space, the orientation of the fabric tensor and the loading direction quickly align in both ACST calculations and DEM tests, which corresponds to the period of loading up to around the peak deviatoric stress ratio (Fig. 6 (c) and (d)).

The good agreement of contact normal fabric evolution between ACST calculations and DEM results in Fig. 6 is aided by the appropriate formulation for the particle orientation fabric tensor evolution as per Eq. (8). Fig. 7 compares the particle orientation fabric tensor norm and orientation of ACST and DEM results. The slower evolution of \mathbf{F}_p compared with that of \mathbf{F}_c is well simulated. In both ACST and DEM results, \mathbf{F}_p begins to evolve significantly only after peak stress is reached, with \mathbf{F}_p

reaching the critical state near the end of the loading process.

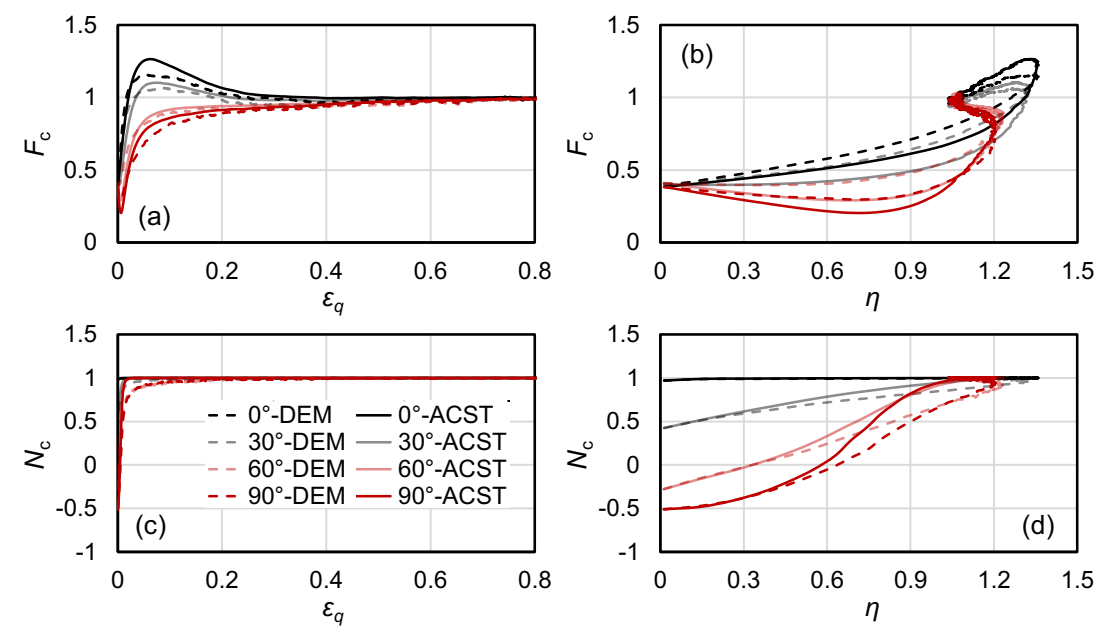


Fig. 6 Contact normal fabric evolution results from drained DEM tests and ACST simulations using Eqs. (7) and (8), for specimens with e_0 =0.656±0.005, and bedding plane angle φ =0°, 30°, 60°, and 90°: (a) F_c - ε_q ; (b) F_c - η ; (c) N_c - ε_q ; (d) N_c - η .

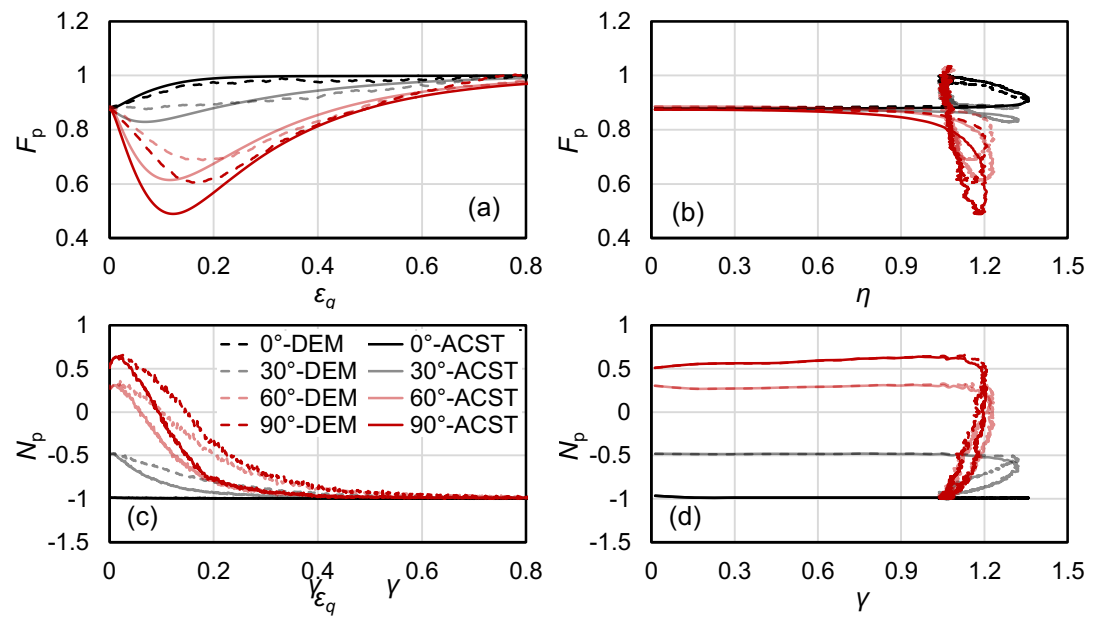


Fig. 7 Particle orientation fabric evolution results from drained DEM tests and ACST simulations using Eqs. (7) and (8), for specimens with e_0 =0.656±0.005, and bedding plane angle φ =0°, 30°, 60°, and 90°: (a) F_p - ε_q ; (b) F_p - η ; (c) N_p - ε_q ; (d) N_p - η .

As explained before, the fabric tensor is not taken from DEM calculations, but is independently obtained from Eq. (7) whose better performance over Eqs. (5) and (6) for the evolution of \mathbf{F}_c results in better simulation of volumetric behaviour in Fig. 8,

compared to that in Fig. 4. The initial contraction tendency of specimens with greater φ is stronger. At high η , the dilatancy-stress relationship begins to converge in the D- η plot (Fig. 8 (a) and (b)), while specimens with smaller φ exhibit stronger peak dilatancy. The anisotropic void ratio development in ACST and DEM results also show good agreement (Fig. 8 (c)).

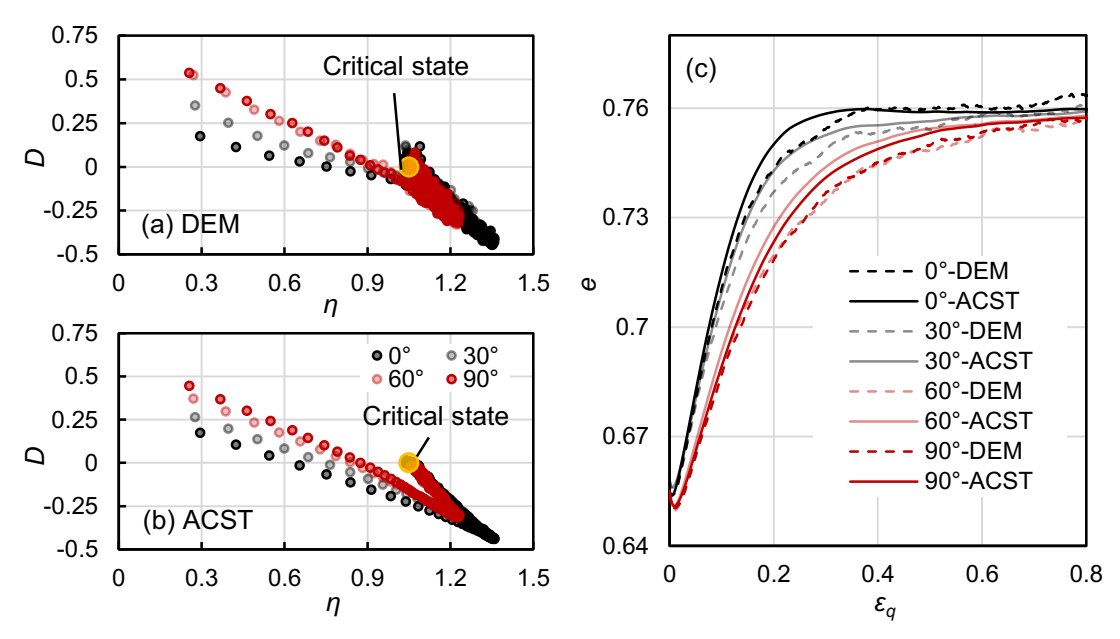


Fig. 8 Dilatancy and void ratio evolution results from drained DEM tests and ACST simulations using Eqs. (7) and (8), for specimens with e_0 =0.656±0.005, and bedding plane angle φ =0°, 30°, 60°, and 90°: (a) *D*-η from DEM; (b) *D*-η from ACST; (c) e- ε_q from DEM and ACST.

4.3 Simulations of DEM drained tests with different void ratio e

Simulations of fabric evolution and volumetric behaviour for specimens with various densities are also conducted using the combined formulation of fabric evolution within ACST, with the same set of parameters in Table 2. Although twelve triaxial tests under b=0 on specimens with e_0 of 0.656 ± 0.005 , 0.690 ± 0.005 , and 0.570 ± 0.005 and φ of 0° , 30° , 60° , and 90° are conducted, Fig. 9 only presents the contact normal and particle orientation fabric tensor norm evolution for four tests for visual clarity, including the tests on specimens with $\varphi=0^{\circ}$ and 90° for the two different initial void

ratios of 0.690 ± 0.005 and 0.570 ± 0.005 . Using the same set of parameters, the evolution of both contact normal and particle orientation fabric tensors during the entire loading process for specimens with drastically different initial densities can be simulated using ACST (Fig. 9). Not only is the greater peak contact normal fabric tensor norm of the dense specimen captured through Eq. (7) (Fig. 9 (a) and (b)), the peak particle orientation fabric tensor norm for the very dense specimen with e_0 =0.570±0.005 and φ =0° is also captured with Eq. (8).

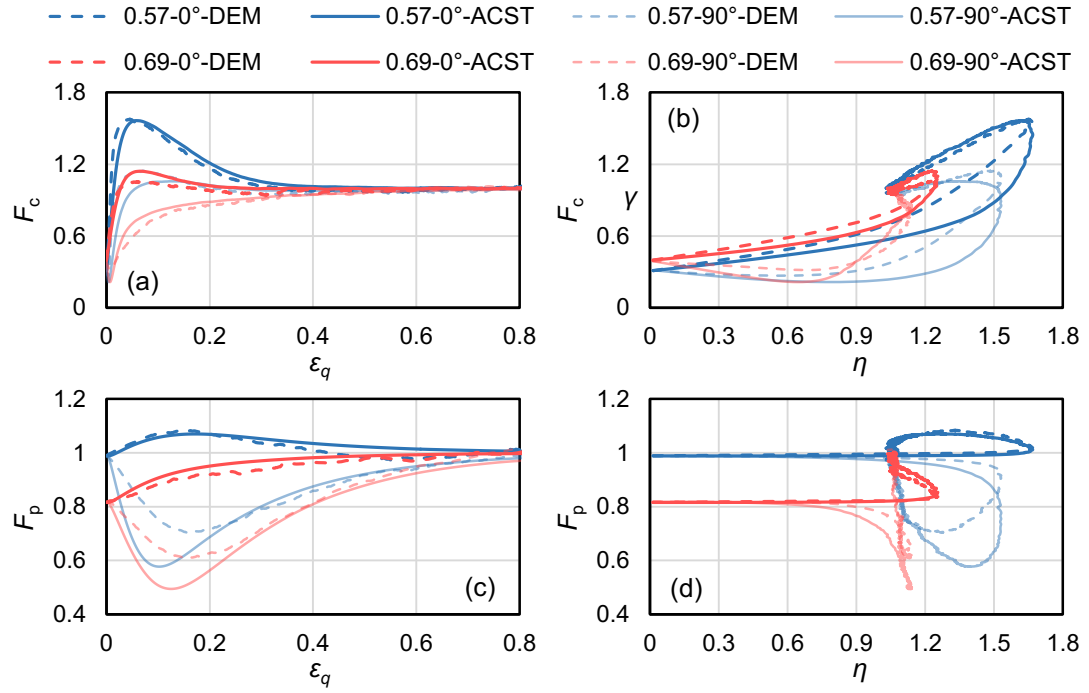


Fig. 9 Contact normal and particle orientation fabric evolution results from drained DEM tests and ACST simulations using Eqs. (7) and (8), for specimens with e_0 =0.570±0.005 and e_0 =0.690±0.005, bedding plane angle φ =0°and 90°: (a) F_c - γ ; (b) F_c - η ; (c) F_p - ε_q ; (d) F_p - η .

Fig. 10 shows the dilatancy and void ratio development results for these tests. The dilatancy results from ACST and DEM agree quantitatively, with looser specimens initially more contractive (Fig. 10 (a) and (b)) and having weaker peak dilatancy. The void ratio development for specimens with different densities is also well simulated using Eqs. (7) and (8) (Fig. 10 (c)). Initially, the looser specimens experience significant

void ratio reduction, while the contraction of the denser specimens are barely visible.

Eventually, specimens with different e_0 end up with the same e_c .

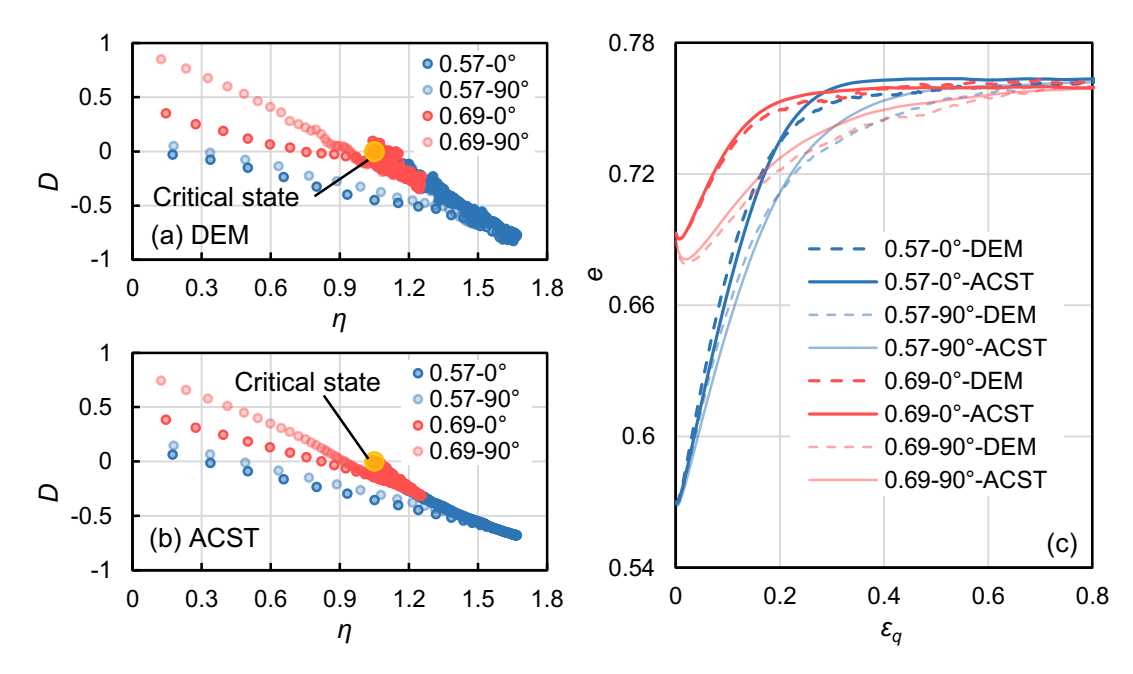


Fig. 10 Dilatancy and void ratio evolution results from drained DEM tests and ACST simulations using in Eqs. (7) and (8), for specimens with e_0 =0.570±0.005 and e_0 =0.690±0.005, bedding plane angle φ =0° and 90°: (a) D- η from DEM; (b) D- η from ACST; (c) e- ε_q from DEM and ACST.

4.4 Simulations of DEM drained tests with different principal stress coefficient b

The results presented in the previous sections are all from tests under triaxial compression with intermediate principal stress coefficient b=0. Here, the performance of the proposed ACST fabric evolution and dilatancy formulation is evaluated for different b values that will have an effect on the values of the FAV $A_c = \mathbf{F}_c$: \mathbf{n} entering Eq. (2) and A_p = \mathbf{F} : \mathbf{n} entering Eq. (7), due to the change of \mathbf{n} . Fig. 11 illustrates the contact normal and particle orientation fabric norm for specimens with e_0 =0.656±0.005 and φ =0°, under b=0, 0.25, 0.5, 0.75, and 1.

The DEM test results for fabric evolution are generally well simulated by the relations of ACST (Fig. 11). Tests with greater b values exhibit lower peak F_c values. However, the difference in peak F_c values is much more pronounced in ACST

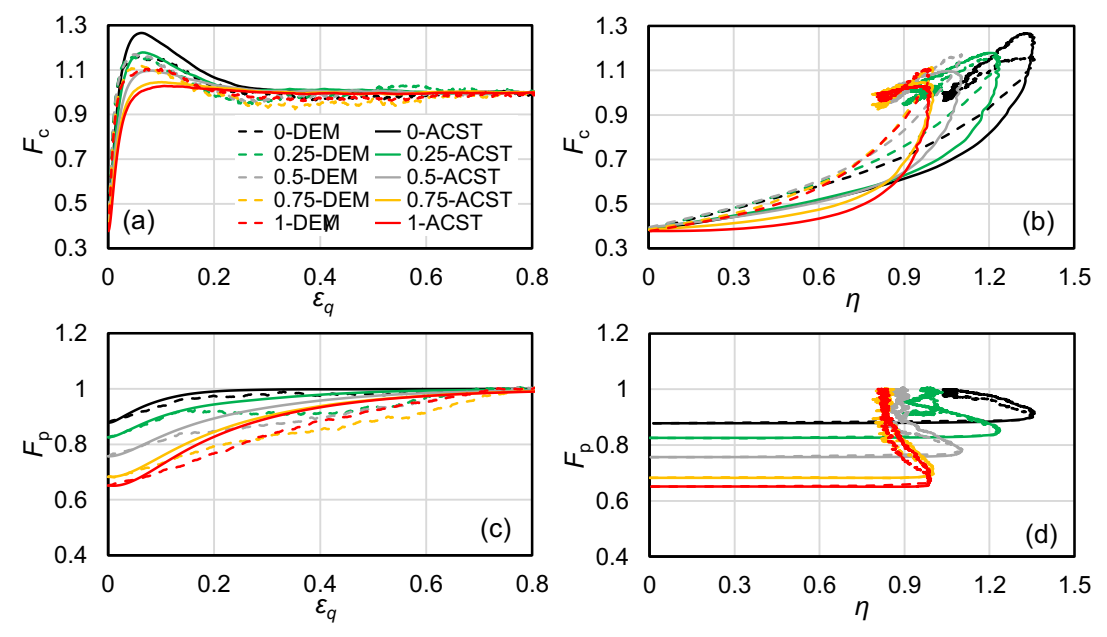


Fig. 11 Contact normal and particle orientation fabric evolution results from drained DEM tests and ACST simulations using Eqs. (7) and (8), for specimens with e_0 =0.656±0.005, under b=0, 0.25, 0.5, 0.75, and 1: (a) F_c - ε_q ; (b) F_c - η ; (c) F_p - ε_q ; (d) F_p - η .

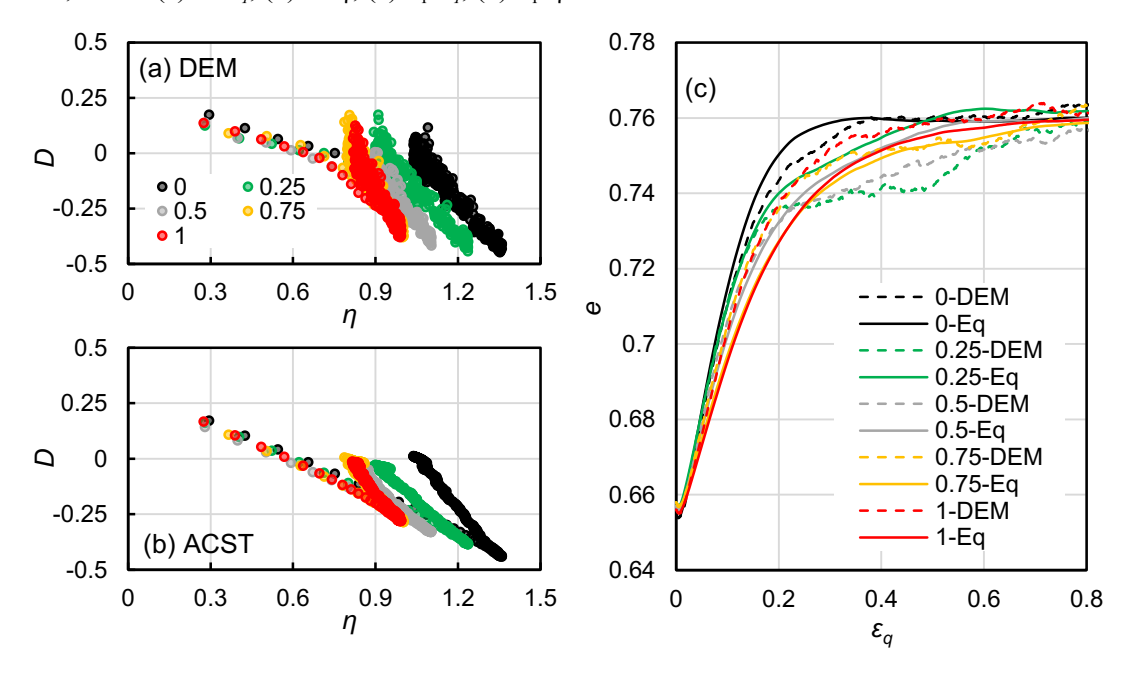


Fig. 12 Dilatancy and void ratio evolution results from drained DEM tests and ACST simulations using Eqs. (7) and (8), for specimens with e_0 =0.656±0.005, under b=0, 0.25, 0.5, 0.75, and 1: (a) D- η from DEM; (b) D- η from ACST; (c) e- ε_q from DEM and ACST.

For the dilatancy simulation results, Fig. 12 (a) and (b) show that the initial dilatancy is almost independent of b in both DEM and ACST. The ACST calculation yields correctly decreasing absolute peak value of D with increasing b, which however

is only slightly observed in the corresponding DEM test results. This may be cause by the over-simplification of Eq. (3) by assuming constant values for d, m, and \hat{e}_A . For void ratio development in Fig. 12 (c), the ACST calculation reflects similar patterns to that of the DEM tests, while overestimating the difference between the tests with different b values up to ε_q of about 0.2 due to the inconsistent simulations for peak dilatancy. After ε_q exceeds 0.2, more fluctuation is observed for the DEM results, possibly due to the limited number of particles. The same critical state void ratio is reached, irrespective of the value of b.

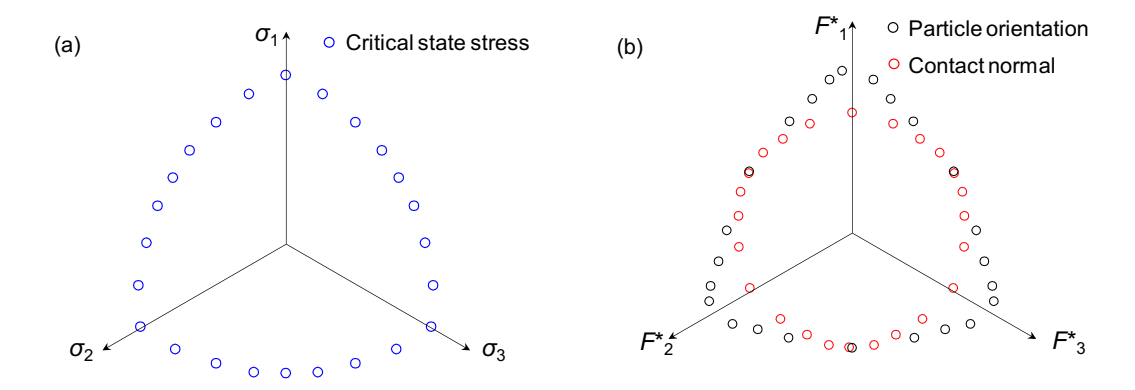


Fig. 13 The DEM results of critical state stress, contact normal fabric, and particle orientation fabric in the π plane for specimens with e_0 =0.657±0.005, under loading with different b values: (a) critical state stress; (b) critical state contact normal and particle orientation fabric (non-normalized).

Both Fig. 11 and 12 indicate that the critical state deviatoric stress ratio M is b dependent (i.e. the well-known Lode angle dependence). Fig. 13 (a) plots the critical state stress in the π plane for the four tests with different b, which follows a typical rounded triangular-shaped surface. DEM tests on spherical particles (Thornton, 2000; Thornton and Zhang, 2010; Zhao and Guo, 2013; Huang et al., 2014; Yuan et al. 2019) showed that the critical state non-normalized contact normal fabric tensor norm is reciprocal to the critical state stress in the π plane, also derived theoretically under certain assumptions (Li and Dafalias, 2015). The non-normalized critical state particle

orientation and contact normal orientation fabric norms for the four tests with different b in this study are plotted in the π plane in Fig. 13 (b). $\mathbf{F}^*_{p,crit}$ is approximately similar in shape to that of $\mathbf{\sigma}_{crit}$ in the π plane, instead of being reciprocal as suggested for $\mathbf{F}^*_{c,crit}$ in the previous studies, because at critical state N^*_{p} = -1 instead of N^*_{c} = 1. Also, \mathbf{F}^*_{c} shows only slight dependency on b in this study, and its reciprocal feature to $\mathbf{\sigma}_{crit}$ plotting is not clearly exhibited. These results indicate that the dependency of critical state fabric on b is different for fabric tensors defined based on different grain scale features and may be more complicated than suggested in Zhao and Guo (2013), especially for non-spherical particles (Yang and Wu, 2016; Nguyen et al., 2018).

4.5 Simulations of DEM undrained tests with different bedding plane angle φ

To further challenge the adaptability of the ACST framework, two undrained DEM tests are conducted on specimens with e_0 =0.655, and bedding plane angles φ =0° and 90°, respectively, and are simulated using the ACST formulations in Eqs. (3), (7), and (8). The exact same parameters as those for the drained tests are used for the simulation of the undrained tests (Table 2). In the drained constant p tests, the critical state void ratio e_c measured in DEM at the particular p can be used as input for ACST calculations. However, in the undrained tests, as p is constantly changing until the critical state, an e_c ~p relationship must be established. In the two undrained tests here, the critical state void ratio e_c =0.655 at p=1180 kPa. The results from drained constant p tests yield e_c =0.761 at p=100 kPa. Using the critical state e_c ~p data under these two conditions, the e_c ~p relationship can be approximated with e_c = e_{c0} - λ_c (p_c / p_a) ξ following Li and Wang (1998), where p_a is the atmospheric pressure, ξ is generally assumed to be

0.7, resulting in back calculated values of 0.784 and 0.023 for e_{c0} and λ_c , respectively. To simulate the p-q stress path of undrained loading, a reasonable approximation for elastic bulk modulus must also be provided in the ACST calculation. Here, it is assumed that that the elastic bulk modulus $K = [(1+e)p_a/\kappa](p/p_a)^{1/2}$ following Richart et al. (1970), with a value of 0.032 for parameter κ , calculated from fitting the elastic bulk modulus obtained through applying hydrostatic stress increments in DEM at various p with contact sliding restricted.

Fig. 14 (a)-(d) show the evolution of the contact normal and particle orientation fabric tensor norms for the two undrained tests from ACST calculations and DEM tests. The evolution of the two fabric tensors during the entire loading process is captured remarkably well, particularly in the plots versus the deviatoric strain, given that no adjustments whatsoever were made to the formulations and parameters used in the drained tests. This further exhibits the general applicability of the combined rate evolution Eqs. (7) and (8) proposed within ACST, as well as the validity of the ACST itself as an appropriate constitutive framework for granular materials.

Recall that in these simulations the deviatoric stress and deviatoric plastic strain variations are inputted from DEM, as shown in Fig. 14 (e), where clear anisotropic behaviour is observed due to large difference in response according to relative orientation of stress and bedding plane. Dilatancy cannot be directly measured during undrained DEM tests, and thus cannot be compared directly with ACST dilatancy results. Instead, the stress path in p-q space for both ACST and DEM are plotted in Fig. 14 (f). The initial decrease in p (indicating contraction), subsequent increase in p

(indicating dilation), and eventual stabilization of stress at the critical state is captured in the ACST calculations. Close up of the early stages of loading in the small window in Fig. 14 (f) shows that the ACST framework is able to simulate the anisotropic volumetric behaviour, i.e. stronger initial contraction tendency of the specimen with greater φ . The anisotropy in deviatoric stress-strain relationship and stress path are consistent with observations in laboratory tests (Symes et al., 1984; Yoshimine et al., 1998).

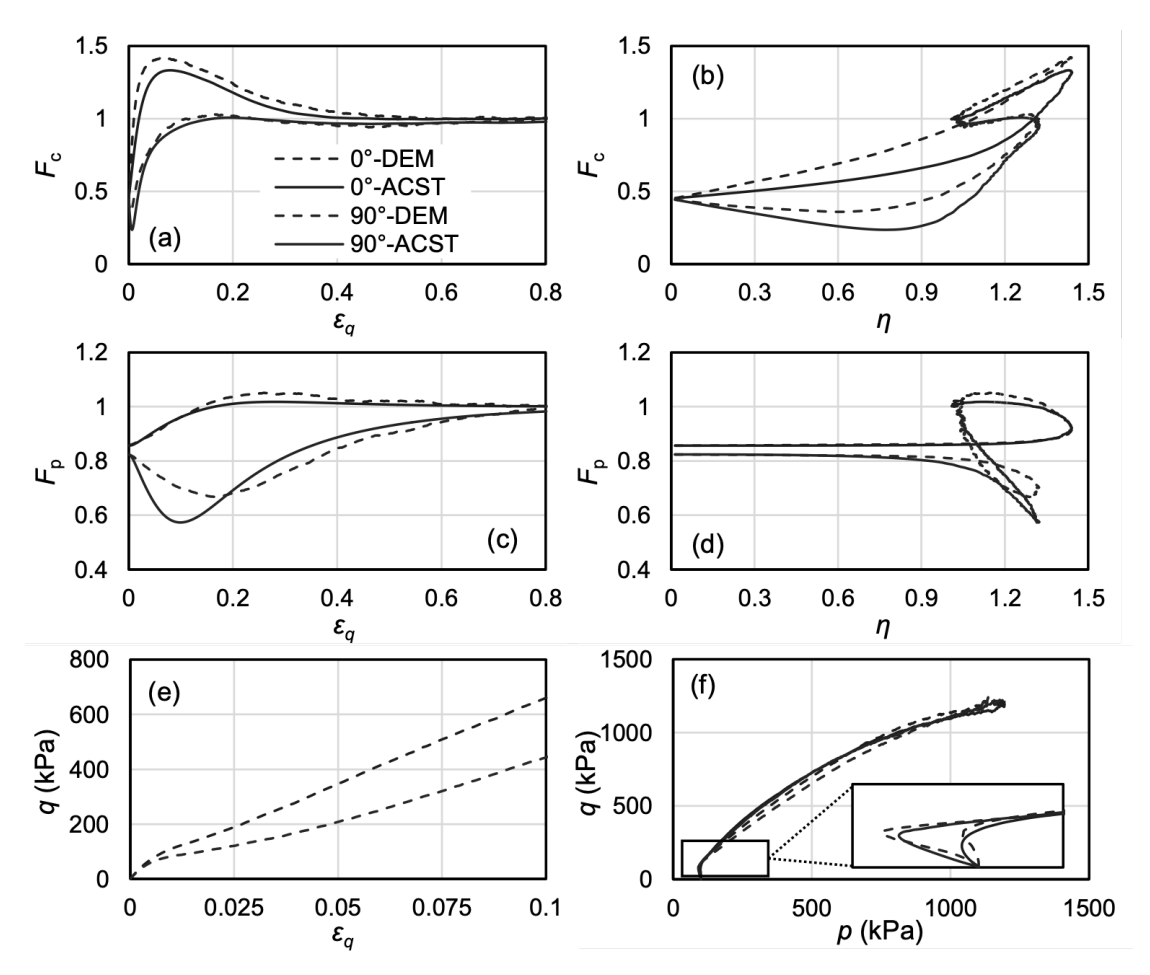


Fig. 14 Fabric and stress evolution results from undrained DEM triaxial tests under b=0 and ACST simulations using Eqs. (9) and (10), for specimens with $e_0=0.655$, bedding plane angle $\varphi=0^\circ$ and 90°: (a) $F_c-\varepsilon_q$; (b) $F_c-\eta$; (c) $F_p-\varepsilon_q$; (d) $F_p-\eta$, (f) $q-\varepsilon_q$ (input from DEM), (f) q-p.

5. Conclusions

The main objectives of this study were to evaluate the validity of two analytical

relations of ACST for the rate equation of evolution of fabric tensor **F** and the dependence of dilatancy on it for granular materials and guide the formulation of the former by comparison with DEM calculations. The DEM tests input the stress ratio and deviatoric plastic strain during loading into these two ACST analytical relations, which then are used to independently calculate fabric evolution and dilatancy, the latter yielding the volumetric deformation. Based on the comparisons of fabric evolution and dilatancy between ACST calculations and DEM tests, it is concluded that the ACST framework is able to address the strongly anisotropic dilatancy response of granular materials and simultaneously capture the evolution of fabric tensor, a confirmation not possible by earlier macroscopic only observations. The contact normal fabric tensor **F**_c can serve as an acceptable grain scale-based fabric going into the ACST framework in determining the dilatancy, a previously assumed fact, but now being firmly confirmed with the following interesting and novel observations.

It was firstly shown that the fabric dependent dilatancy is relatively sensitive to the exactness with which the contact normal fabric tensor is analytically calculated. The peak contact normal-fabric norm, before reaching its lower critical state value for dense materials under triaxial loading, was found to be related to dilatancy based on DEM results. In addition, the evolution of the contact normal fabric tensor was observed to be influenced by the also evolving particle orientation fabric tensor as well. Therefore, the incorporation of the combined influence of dilatancy and particle orientation fabric in the expression for the coefficient r of the original Eq. (4) proposed by Li and Dafalias (2012), entering the contact normal fabric rate evolution Eq. (7) in conjunction with Eq.

(8), is an important and original proposition of this work, called the combined formulation. This combined formulation is shown to achieve good analytical description of contact normal fabric evolution and dilatancy anisotropy in a very wide range of loadings. Both drained and undrained loadings were considered, always with the same set of model constants. For the drained loadings in particular, the responses of three different categories of samples were simulated, namely those with different bedding plane orientations, different initial void ratios and different intermediate principal stress coefficient *b*.

Some issues still remain in regard to the effect of b. The simulated peak dilatancy was found to be slightly inconsistent with DEM observations for tests with different values of b, resulting in overestimation of the influence of b on fabric and void ratio evolution. The dependency of critical state fabric on b was also found to be different for contact normal and particle orientation-based fabric tensors associated with non-spherical particles. To address these issues further analysis should be carried out on the dilatancy of granular materials under 3D loading with different b.

Acknowledgments:

Rui Wang would like to thank the National Natural Science Foundation of China (No. 51708332) and Tsinghua University Initiative Scientific Research Program (2019Z08QCX01) for funding this work. Pengcheng Fu's contribution was performed under the auspices of the U.S. Department of Energy by Lawrence Livermore National Laboratory under Contract DE-AC52-07NA27344. This work is LLNL report LLNL-JRNL-783568. Y. F. Dafalias acknowledges support by the European Research Council under the European Union's Seventh Framework program (FP7/2007-2013)/ERC

- 644 IDEAS Advanced Grant Agreement 290963 (SOMEF), the General Secretariat for
- Research and Technology of Greece (Matching Funds Program) under the project titled
- "SOFI SOil Fabric Investigation" and by the European Regional Development Fund
- 647 under Grant No. CZ.02.1.01/0.0/0.0/15 003/0000493 CeNDYNMAT, Czech
- 648 Republic.

649

650 References

- Bagi, K., 1996. Stress and strain in granular assemblies. Mechanics of Materials 22(3), 165-
- Been, K., Jefferies, M. G., 1985. A state parameter for sands. Géotechnique 35(2), 99-112.
- Cao, W., Wang, R., Zhang, J.M., 2016. Formulation of anisotropic strength criteria for cohesionless granular materials. International Journal of Geomechanics 17 (7), 04016151.
- Cundall, P.A. Strack, O.D., 1979. A discrete numerical model for granular assemblies. Géotechnique 29(1), 47-65.
- Dafalias, Y.F., 2016. Must critical state theory be revisited to include fabric effects? Acta Geotechnica 11(3), 479-491.
- Dafalias, Y.F., Manzari, M.T., 2004. Simple plasticity sand model accounting for fabric change effects. Journal of Engineering Mechanics 130(6), 622-634.
- Dafalias, Y.F., Papadimitriou, A.G., Li, X.S., 2004. Sand plasticity model accounting for inherent fabric anisotropy. Journal of Engineering Mechanics 130(11), 1319-1333.
- Fu, P. and Dafalias, Y.F., 2011. Fabric evolution within shear bands of granular materials and its relation to critical state theory. International Journal for Numerical and Analytical Methods in Geomechanics 35(18), 1918-1948.
- Fu, P., Dafalias, Y.F., 2012. Quantification of large and localized deformation in granular materials. International Journal of Solids and Structures, 49(13), 1741-1752.
- Gao, Z.W, Zhao, J.D, Li, X.S., Dafalias, Y.F., 2014. A critical state sand plasticity model accounting for fabric evolution. International journal for numerical and analytical methods in geomechanics 38(4), 370-390.
- Guo, P., 2008. Modified direct shear test for anisotropic strength of sand. Journal of Geotechnical and Geoenvironmental Engineering 134(9), 1311-1318.
- Guo, N., Zhao, J., 2013. The signature of shear-induced anisotropy in granular media. Computers and Geotechnics 47, 1–15.
- Hu, N., Yu, H.-S., Yang, D. H., Zhuang, P. Z., 2019. Constitutive modelling of granular materials using a contact normal-based fabric tensor. Acta Geotechnica, 10.1007/s11440-019-00811-z0123456
- Huang, X., Hanley, K.J., O'Sullivan, C., Kwok, C.Y. and Wadee, M.A., 2014. DEM analysis of the influence of the intermediate stress ratio on the critical-state behaviour of granular materials. Granular Matter, 16(5), 641-655.

- Kuhn, M.R., Renken, H.E., Mixsell, A.D., Kramer, S.L., 2014. Investigation of Cyclic Liquefaction with Discrete Element Simulations. Journal of Geotechnical and Geoenvironmental Engineering 140(12), 04014075
- Lashkari, A., Khodadadi, M., Binesh, S.M., Rahman, M.M., 2019. Instability of Particulate Assemblies under Constant Shear Drained Stress Path: DEM Approach. International Journal of Geomechanics, 19(6), 04019049.
- Li, X., Li, X.S., 2009. Micro-macro quantification of the internal structure of granular materials. Journal of Engineering Mechanics 135(7), 641-656.
- Li, X.S., Dafalias, Y.F., 2000. Dilatancy for cohesionless soils. Geotechnique 50(4): 449–460.
- Li, X.S., Dafalias, Y.F., 2002. Constitutive modeling of inherently anisotropic sand behavior. Journal of Geotechnical and Geoenvironmental Engineering 128(10), 868-880.
- Li, X.S., Dafalias, Y.F., 2012. Anisotropic critical state theory: role of fabric. Journal of Engineering Mechanics 138(3), 263-275.
- Li, X.S., Dafalias, Y.F., 2015. Dissipation consistent fabric tensor definition from DEM to continuum for granular media. Journal of the Mechanics and Physics of Solids 78, 141-153.
- Li, X.S., Wang, Y., 1998. Linear representation of steady-state linefor sand. Journal of Geotechnical and Geoenvironmental Engineering 124(12), 1215–1217.
- Manzari, M.T., Dafalias, Y.F., 1997. A critical state two-surface plasticity model for sands. Geotechnique, 47(2), 255-272.
- MiDi, G.D.R., 2004. On dense granular flows. The European Physical Journal E 14(4), 341-365.
- Nguyen, H.B.K., Rahman, M.M., Fourie, A.B., 2018. Characteristic behavior of drained and undrained triaxial compression tests: DEM study. Journal of Geotechnical and Geoenvironmental Engineering, 144(9), 04018060.
- Oda, M., 1972. The mechanism of fabric changes during compressional deformation of sand. Soils and foundations 12(2), 1-18.
- Oda, M., 1993. Inherent and induced anisotropy in plasticity theory of granular soils. Mechanics of Materials 16 (1–2), 35–45.
- Papadimitriou, A.G., Chaloulos, Y.K., Dafalias, Y.F., 2018. A fabric-based sand plasticity model with reversal surfaces within anisotropic critical state theory. Acta Geotechnica.
- Petalas, A.L., Dafalias, Y.F., Papadimitriou, A.G., 2019. SANISAND FN: An evolving fabric based sand model accounting for stress principal axes rotation. International Journal for Numerical and Analytical Methods in Geomechanics 43(1), 97-123.
- Richart, F.E., Jr., Hall, J.R., Woods, R.D., 1970. Vibrations of soils and foundations. Prentice-Hall, Inc., Englewood Cliffs, N.J.
- Roscoe, K.H., Schofield, A.N., Wroth, C.P., 1958. On the yielding of soils. Geotechnique 8(1), 22-53.
- Rowe, P. W., 1962. The stress-dilatancy relation for static equilibrium of an assembly of particles in contact. Proceedings of the Royal Society of London. Series a. Mathematical and Physical Sciences, 269(1339), 500-527.
- Satake M., 1982. Fabric tensor in granular materials. Amsterdam: Proceedings of the IUTAM Symposium on Deformation and Failure of Granular Materials, 63-68.

- Schofield, A.N., Wroth, C.P., 1968. Critical state soil mechanics. McGraw-Hill, London.
- Shi, J., Guo, P., 2018. Fabric evolution of granular materials along imposed stress paths. Acta Geotechnica, 13(6), 1341-1354.
- Šmilauer, V., Catalano, E., Chareyre, B., Dorofeenko, S., Duriez, J., Gladky, A., Kozicki, J., Modenese, C., Scholtès, L., Sibille, L., Stránský, J., 2015. Yade Documentation 2nd ed. The Yade Project. DOI 10.5281/zenodo.34073 (http://yade-dem.org/doc/)
- Symes, M.J.P.R., Gens, A. and Hight, D.W., 1984. Undrained anisotropy and principal stress rotation in saturated sand. Geotechnique, 34(1), 11-27.
- Theocharis, A.I., Vairaktaris, E., Dafalias, Y.F., Papadimitriou, A.G., 2017. Proof of incompleteness of critical state theory in granular mechanics and its remedy. Journal of Engineering Mechanics 143(2), 04016117.
- Theocharis, A.I., Vairaktaris, E., Dafalias, Y.F., Papadimitriou, A.G., 2019. Necessary and sufficient conditions for reaching and maintaining critical state. International Journal for Numerical and Analytical methods in Geomechanics; 1-15. DOI: 10.1002/nag.2943.
- Thornton, C., 2000. Numerical simulations of deviatoric shear deformation of granular media. Géotechnique, 50(1), 43-53.
- Thornton, C., Zhang, L., 2010. On the evolution of stress and microstructure during general 3D deviatoric straining of granular media. Géotechnique, 60(5), 333-341.
- Tobita, Y., 1989. Fabric tensors in constitutive equations for granular materials. Soils and Foundations 29(4), 91-104.
- Tong, Z., Fu, P., Zhou, S., Dafalias, Y.F., 2014. Experimental investigation of shear strength of sands with inherent fabric anisotropy. Acta Geotechnica 9(2), 257-275.
- Ueda, K., Iai, S., 2019. Constitutive modeling of inherent anisotropy in a strain space multiple mechanism model for granular materials. International Journal for Numerical and Analytical Methods in Geomechanics, 43(3), 708-737.
- Wan R. C. Guo P. J., 2001. Stress dilatancy and fabric dependencies on sand behavior. Journal of Engineering Mechanics, 130(6), 1106-1116.
- Wan R. C. Guo P. J., 2004. Drained cyclic behaviour of sand with fabric dependence. Journal of Engineering Mechanics, 127(11), 635-645.
- Wan, R. Pinheiro, M., 2014. On the validity of the flow rule postulate for geomaterials. International Journal for Numerical and Analytical Methods in Geomechanics 38(8), 863-880.
- Wang, R., Cao, W., Zhang, J.M., 2019 a. Dependency of dilatancy ratio on fabric anisotropy in granular materials. Journal of Engineering Mechanics, 10.1061/(ASCE)EM.1943-7889.0001660.
- Wang, R., Fu, P., Zhang, J.M., Dafalias, Y.F., 2016. DEM study of fabric features governing undrained post-liquefaction shear deformation of sand. Acta Geotechnica 11(6), 1321-1337.
- Wang, R., Fu, P., Zhang, J.M., Dafalias, Y.F., 2017. Evolution of various fabric tensors for granular media towards the critical state. Journal of Engineering Mechanics 143(10), 04017117-1-9.
- Wang, R., Fu, P., Zhang, J.M., Dafalias, Y.F. 2019 b. Fabric characteristics and processes influencing the liquefaction and re-liquefaction of sand. Soil Dynamics and Earthquake Engineering 10.1016/j.soildyn.2019.105720.

- Wang, R., Zhang, J.M., Wang, G., 2014. A unified plasticity model for large post-liquefaction shear deformation of sand. Computers and Geotechnics 59, 54-66.
- Woo, S. I., Salgado, R., 2015. Bounding surface modeling of sand with consideration of fabric and its evolution during monotonic shearing. International Journal of Solids and Structures 63, 277-288.
- Wu, W., 1998. Rational approach to anisotropy of sand. International Journal for Numerical and Analytical Methods in Geomechanics 22(11), 921-940.
- Xue L., Kruyt N. P., Wang R., Zhang J.M., 2019. 3D DEM simulation of principal stress rotation in different planes of cross-anisotropic granular materials. International Journal for Numerical and Analytical Methods in Geomechanics, 10.1002/nag.2945.
- Yang, Z.X., Wu, Y., 2016. Critical state for anisotropic granular materials: a discrete element perspective. International Journal of Geomechanics 17(2), 04016054.
- Yang, Z.X., Xu, T.T., Chen, Y.N, 2018. Unified Modeling of the Influence of Consolidation Conditions on Monotonic Soil Response Considering Fabric Evolution. Journal of Engineering Mechanics 144(8), 04018073.
- Yao, Y., Tian, Y., Gao, Z., 2017. Anisotropic UH model for soils based on a simple transformed stress method. International Journal for Numerical and Analytical Methods in Geomechanics 41(1), 54-78.
- Yoshimine, M., Ishihara, K., Vargas, W., 1998. Effects of principal stress direction and intermediate principal stress on undrained shear behavior of sand. Soils and Foundations 38(3), 179-188.
- Yuan, R., Yu, H.S., Yang, D.S., Hu, N., 2019. On a fabric evolution law incorporating the effects of b-value. Computers and Geotechnics, 105, 142-154.
- Zhao, J., Gao, Z., 2016. Unified anisotropic elastoplastic model for sand. Journal of Engineering Mechanics 142(1), 04015056.
- Zhao, J., Guo, N., 2015. The interplay between anisotropy and strain localisation in granular soils: a multiscale insight. Géotechnique 65 (8), 642-656.

651

652

Appendix

- Referring to Eq. (7), the parameter β is expected to be related to particle elongation or
- aspect ratio R and other factors. For spherical particles, where particle orientation is
- non-existent resulting in isotropic fabric, hence, $\mathbf{F}_p = \mathbf{0}$ and $A_p = 0$, β should be set equal
- to 0 so that $\mathbf{F}_c = \mathbf{n}$ from Eq. (7) at critical state where D = 0. One may assume in fact
- that β is a continuous function of aspect ratio R such that $\beta = 0$ when R=1. This
- guarantees the necessary continuity of the quantity $\beta(1+A_p)$ at R=1 in Eq. (7), because
- the \mathbf{F}_p and A_p may change discontinuously from their 0 values at R=1. This may happen
- if for example one considers an arrangement of particles shown in Fig. 5 with such
- particles changing from spherical with R=1 and $\mathbf{F}_p = \mathbf{0}$, to non-spherical with $R\neq 1$ and

 $\mathbf{F}_p \neq \mathbf{0}$ for any value of R as close or as far from 1.

In order to check the validity of the requirement to set $\beta=0$ when R=1, two DEM tests on spherical particles are conducted and used Eq. (7) with $\beta=0$ in ACST simulations. Due to the change in material, the critical state and fabric evolution rate changed, thus requiring re-calibration of all parameters. The figure below compares the contact normal fabric evolution void ratio development under these circumstances. Good agreement between ACST and DEM is achieved with only Eq. (7) and $\beta=0$, without of course the use of Eq. (8) that has no meaning for spherical particles.

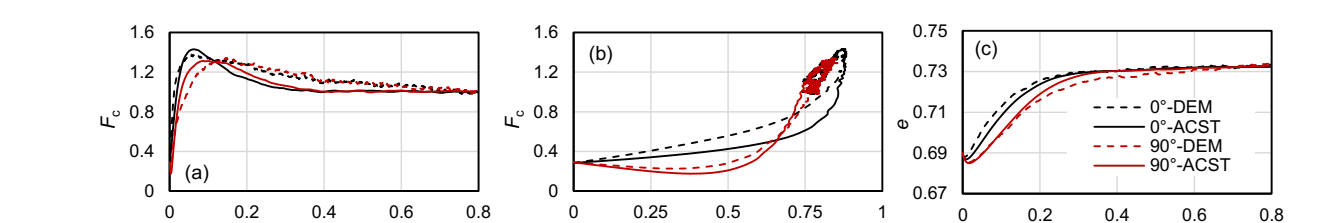


Fig. 15 Contact normal fabric evolution and void ratio development results from drained DEM tests and ACST simulations using Eq. (7) and $\beta = 0$, on two specimens consisting of spherical particles with different bedding plane angles.